AIP | Journal of Applied Physics

Griffiths phase-like behavior and spin-phonon coupling in double perovskite Tb2NiMnO6

Harikrishnan S. Nair, Diptikanta Swain, Hariharan N., Shilpa Adiga, Chandrabhas Narayana et al.

Citation: J. Appl. Phys. **110**, 123919 (2011); doi: 10.1063/1.3671674
View online: http://dx.doi.org/10.1063/1.3671674
View Table of Contents: http://jap.aip.org/resource/1/JAPIAU/v110/i12
Published by the American Institute of Physics.

Griffiths phase-like behavior and spin-phonon coupling in double perovskite Tb_2NiMnO_6

Harikrishnan S. Nair,[1,a)] Diptikanta Swain,[2] Hariharan N.[3] Shilpa Adiga,[1] Chandrabhas Narayana,[2] and Suja Elzabeth[3]
[1]*Jülich Center for Neutron Sciences-2/Peter Grünberg Institute-4, Forschungszentrum Jülich GmbH, 52425 Jülich, Germany*
[2]*Chemistry and Physics of Materials Unit, Jawaharlal Nehru Centre for Advanced Scientific Research, Bangalore 560064, India*
[3]*Department of Physics, C. V. Raman Avenue, Indian Institute of Science, Bangalore 560012, India*

(Received 5 October 2011; accepted 10 November 2011; published online 29 December 2011)

The Griffiths phase-like features and the spin-phonon coupling effects observed in Tb_2NiMnO_6 are reported. The double perovskite compound crystallizes in monoclinic $P2_1/n$ space group and exhibits a magnetic phase transition at $T_c \sim 111$ K as an abrupt change in magnetization. A negative deviation from ideal Curie–Weiss law exhibited by $1/\chi(T)$ curves and less-than-unity susceptibility exponents from the power-law analysis of inverse susceptibility are reminiscent of Griffiths phase-like features. Arrott plots derived from magnetization isotherms support the inhomogeneous nature of magnetism in this material. The observed effects originate from antiferromagnetic interactions that arise from inherent disorder in the system. Raman scattering experiments display no magnetic-order-induced phonon renormalization below T_c in Tb_2NiMnO_6, which is different from the results observed in other double perovskites and is correlated to the smaller size of the rare earth. The temperature evolution of full-width-at-half-maximum for the *stretching* mode at 645 cm^{-1} presents an anomaly that coincides with the magnetic transition temperature and signals a close connection between magnetism and lattice in this material. © *2011 American Institute of Physics*. [doi:10.1063/1.3671674]

I. INTRODUCTION

Double perovskites $R_2BB'O_6$ (R = rare earth; B, B' = transition metal) are interesting systems owing to the variety of phenomena they display including large magnetocapacitance, magnetoresistance, cationic ordering, high temperature structural phase transitions, and predicted multiferroic properties.[1–5] One of the most studied double perovskite, La_2NiMnO_6, displays large, magnetic-field-induced changes in resistivity and dielectric constant at 280 K—a temperature much higher than previously reported for such couplings.[1] The combination of multiple functionalities with magnetic, dielectric, and lattice degrees of freedom makes double perovskites a material of current interest with device application potential.[6,7] $R_2BB'O_6$ compounds are reported to crystallize either in monoclinic $P2_1/n$ space group, in which case, layers of B^{2+} and B'^{4+} alternate periodically or in orthorhombic $Pbnm$ structure where B^{3+} and B'^{3+} are randomly distributed in the lattice.[2,8] Most of the ordered double perovskites exhibit ferromagnetism (FM), which originates from the superexchange interaction between ordered B^{2+} and B'^{4+} ions.[1,9,10] In ordered La_2NiMnO_6, the Ni^{2+} ($t_{2g}^5 e_g^4$)-O-Mn^{4+} ($t_{2g}^3 e_g^0$) magnetic exchange leads to prominent ferromagnetic interactions. However, even in the ordered state, certain percentage of B and B' cations interchanges their respective crystallographic positions leading to what is known as *antisite disorder* in these materials. Monte Carlo simulations as well as experimental investigations have revealed that this disorder markedly influences the magnetic properties and can lead to secondary magnetic phases at low temperature.[8,11,12] Antisite disorder can introduce additional antiferromagnetic exchange interactions in the form of Ni^{2+} -O-Ni^{2+} or Mn^{4+} -O-Mn^{4+}; this can result in reduction of ferromagnetic saturation magnetization, and such interactions, which get modulated by cationic size mismatch at the La site, have been observed through magnetic measurements on La_2NiMnO_6.[12] It must be noted that short range ferromagnetic correlations above T_c have been observed in La_2NiMnO_6, confirmed by the anomalous softening of phonon modes due to spin-phonon coupling, which extended up to high temperatures.[13–15] X ray magnetic circular dichroism studies revealed clear signals above T_c in La_2NiMnO_6, indicating the presence of short-range FM correlations.[14] Majority of the existing literature on double perovskites addresses La-based systems, whereas the effects of smaller, heavier magnetic rare earth at the R site have received less attention. Recently, investigations on a series of R_2NiMnO_6 compounds found that the Ni-O-Mn bond length and bond angle, which are directly involved in superexchange interactions, are significantly modified with reduction in R-size.[16] As a consequence, multiple magnetic interactions can develop in the system and lead to inhomogeneous magnetic states similar to the clustered or phase separated states observed in perovskite manganites. To strike a comparison with the case of manganites, quenched disorder arising from the random distribution of cations of different sizes and charges introduces phase inhomogeneity through size mismatch of cations and bond disorder of the Mn-O-Mn network, thereby paving the way for Griffiths phase.[17,18] Many manganites exhibit Griffiths phase-like feature, for example, $(La_{1-y}Pr_y)_{0.7}Ca_{0.3}Mn^{16/18}O_3$,[19]

a)Electronic addresses: h.nair@fz-juelich.de and krishnair1@gmail.com.

$Sm_{0.5}Sr_{0.5}MnO_3$ nanomanganites,[20] and $Pr_{0.5}Sr_{0.5}Mn_{1-y}Ga_yO_3$.[21] The cationic disorder arising from the mixed occupancy at the *B* site and the smaller size of the rare earth could lead to similar effects in double perovskites.

The phonon spectra of double perovskites have been actively investigated using Raman spectroscopy methods, for example, in La_2CoMnO_6 and La_2CoMnO_6 bulk and thin films.[7,22–24] Strong spin-phonon coupling has been reported in single crystals and epitaxial thin films of La_2NiMnO_6.[13,25] The effect of cationic size of the rare earth on the phonon properties has not been investigated yet. In a recent Raman study on Pr_2NiMnO_6, Truong *et al.* observed that with a smaller rare earth than La at the *R* site, the spin-phonon coupling is weakened and the physical properties of rare earth double perovskite were a function of the type of *R*.[26] Recent theoretical prediction[5] about the multiferroicity in Y_2NiMnO_6 also points toward the importance of the type of *R* in double perovskites. It was found theoretically that changing *R* from La to Y drives the ground state from ferromagnetic to antiferromagnetic *E** type, which breaks inversion symmetry generating electric polarization. It is, therefore, rewarding to investigate the magnetic and phonon properties of double perovskites upon change in ionic size of *R*. In this report, we present the results of detailed magnetization and Raman scattering experiments on Tb_2NiMnO_6 to explore the effect of substituting a magnetic rare earth at the *R* site on the magnetism and spin-phonon coupling.

II. EXPERIMENTAL SECTION

Polycrystalline Tb_2NiMnO_6 used in the present study was prepared by conventional solid state synthesis. The precursors Tb_2O_3, NiO, and MnO_2 (3N purity or higher) weighted in stoichiometric amounts were mixed and ground together in a mortar and was heat treated initially at 1000°C for 24 h and further at 1300°C for 36 h, after re-grinding. Powder x ray diffractogram (PXD) was obtained by a Philips X'pert diffractometer (Cu K_α) and was analyzed by Rietveld method[27] using FULLPROF suite of programs.[28] Temperature dependent dc magnetization measurements were performed in a commercial SQUID magnetometer (Quantum Design) in zero field-cooled (ZFC) and field-cooled (FC) cycles with applied fields of 20, 100, 500, 20, and 40 kOe. In addition, at 20 Oe, field-cooled warming/cooling (FCW/FCC) curves were also recorded. Raman scattering experiments were performed in a custom-built Raman spectrometer[29] using a 532 nm frequency-doubled solid state Nd-YAG laser with 8 mW power. The measurements were carried out in back scattering geometry in the temperature range 77-300 K.

III. RESULTS AND DISCUSSION

The crystal structure of Tb_2NiMnO_6 (TNMO) was refined in monoclinic space group $P2_1/n$ (space group no.: 14) with an agreement factor, $\chi^2 = 3.74$. The refined lattice parameters obtained from the analysis, $a = 5.2699(2)$ Å, $b = 5.5425(7)$ Å and $c = 7.5251(2)$ Å and the monoclinic angle $\beta = 89.79°$ are in reasonable agreement with the previous report.[16] The results are presented in Fig. 1 along

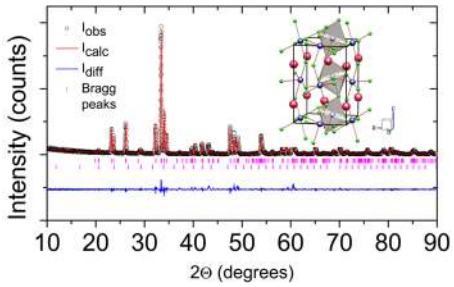

FIG. 1. (Color online) The experimental x ray diffraction pattern of Tb_2NiMnO_6 along with the results of Rietveld analysis. A minor impurity phase of Tb_2O_3 was identified and quantified as 4 wt. %. The inset presents a schematic of the crystal structure in monoclinic $P21/n$ space group. The large pink spheres represent Tb the small green ones are oxygen. The network of corner-sharing octahedra is indicated with N/Mn at the center of the octahedra.

with a structural diagram depicting the schematic of the crystal structure. A minor impurity phase of Tb_2O_3 (4 wt. %) was identified in the x ray pattern. The structural parameters and selected bond distances and angles from the analysis are presented in Table I. The crystal structure adopted by $R_2BB'O_6$ compounds depends on cationic size, charge, and the *R*/*B* radius ratio, which are empirically quantified in tolerance factor. A monoclinic unit cell is favored if the tolerance factor, $t = ((r_R + r_{R'})/2 + r_o)/\sqrt{2}((r_B + r_{B'})/2 + r_o)$ (where r_R, r_B, and r_o are ionic radii of rare earth, transition metal, and oxygen, respectively), is less than unity. With a $t = 0.858$, a monoclinic unit cell is empirically expected for TNMO (the ionic radii values for calculating *t* were taken from Ref. 30). The bond distances and angles obtained from the structural refinement compiled in Table I are comparable to the reported values of Ni^{2+}-O and Mn^{4+}-O distances,[16] thereby indicating a nearly ordered Ni^{2+}/Mn^{4+} arrangement. A quantitative estimate of the valence states of the cations was obtained by calculating the bond valence sums (BVS). The calculated values, presented in Table I compare well with those reported for Mn_{4+}-O and Ni^{2+}-O bonds, thereby supporting a predominant Ni^{2+}/Mn^{4+} cationic arrangement for TNMO.

The *M*(*ZFC*) and *M*(*FC*) magnetization curves of Tb_2NiMnO_6 at applied field of 100 Oe are presented in the main panel of Fig. 2 while the insets 2(a) and 2(b) show the same curves at higher applied fields of 500 and 20 kOe, respectively. The *ZFC* and *FC* arms in Fig. 2 show a split at the magnetic transition temperature, $T_c \cong 111$ K where the system enters a magnetically ordered state. On increasing the

TABLE I. The structural parameters and selected bond distances and bond angles of Tb_2NiMnO_6 at room temperature. The atomic positions were Tb 4*e*(x,y,z), Ni 2*c*(0.5,0,0.5), Mn 2*d*(0.5,0,0), and O 4*e*(x,y,z). *TM* stands for the transition metal at the *B* site, Co, or Mn. BVS indicates bond valence sum values.

Space group	$P2_1/n$
Space group number	14
Lattice parameters	$a = 5.2699(2)$ Å, $b = 5.5425(7)$ Å, $c = 7.5251(2)$ Å, $= 89.79°$
Bond distance	*TM*-O ≈ 1.99 Å
Bond angle	*TM*-O1-*TM* ≈ 140°
BVS	Tb = 3.6, Ni = 2.4, Mn = 4.1

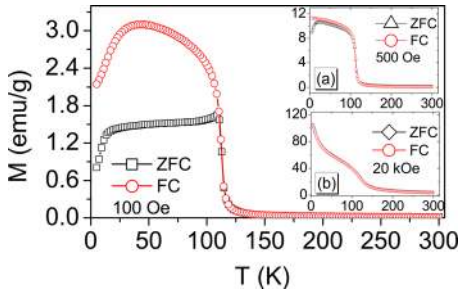

FIG. 2. (Color online) Main panel: The ZFC and FC magnetization curves of Tb_2NiMnO_6 at 100 Oe. The magnetic transition is evident at $T_c \sim 111$. Insets (a) and (b) show the ZFC and FC curves at 500 and 20 kOe, respectively.

applied magnetic field, the *ZFC*/*FC* arms begin to merge, and at 20 kOe, complete merging is attained. With the application of a magnetic field, the magnetization at low temperature is enhanced, typical of systems with a ferromagnetic component. At low applied fields, the $M(ZFC)$ shows a downturn below ≈15 K, which decreases as the applied field increases to 20 kOe. Other double perovskites like Nd_2CoMnO_6 display such a downturn that originates from the anti-parallel alignment of rare earth moment with respect to the Ni/Mn moments.[31]

The transition temperature observed in magnetization measurements was confirmed through specific heat, $C_p(T)$ as presented in Fig. 3, where a peak was observed at 111 K. Apart from the peak at T_c and a low temperature hump that arises from the Schottky effect, the C_p displays no anomalies or peaks from any impurities. The analysis of low temperature C_p was performed by assuming a polynomial expansion, $C_p = \gamma T + \beta_3 T^3 + \beta_5 T^5 + \beta_7 T^7$. Our fitting gave $\gamma = 0.42$ mJ/mol K^2 for the linear term and $\beta_3 = 6.2 \times 10^{-7}$/mol K^4 for the lattice term. The γ value observed in Tb_2NiMnO_6 is smaller than the value observed in $La_{0.4}Ca_{0.6}MnO_3$ manganite showing Griffiths phase-like properties.[32] The low value for γ also suggests a low contribution from electronic conduction in this insulating double perovskite.

In the main panel of Fig. 4, the $\chi(T)$ plots at different applied magnetic fields of 20 Oe, 500 Oe, 20 kOe, and 40 kOe derived from dc magnetization measurements are presented. The downturn observed in the $1/\chi(T)$ curves is reminiscent of systems described by Griffiths phase (GP),[17,18] which was originally proposed for randomly diluted Ising

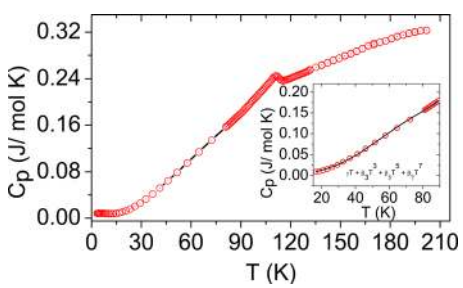

FIG. 3. (Color online) Main panel: The specific heat of Tb_2NiMnO_6 confirming the phase transition of the Ni/Mn lattice at $T_c \sim 111$ K. A broad hump-like feature is observed at low temperature, which is related to Schottky effect. The inset represents the fit to the low temperature C_p assuming a polynomial expansion in powers of T.

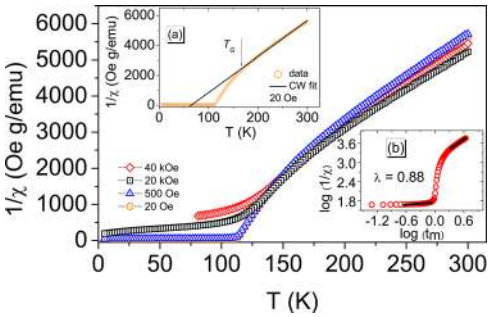

FIG. 4. (Color online) Main panel: The inverse susceptibility $1/\chi(T)$ at different applied fields 20 Oe, 500 Oe, 20 kOe, and 40 kOe. As the applied magnetic field increases, the downward deviation is suppressed. The inset (a) presents the CW analysis of $1/\chi(T)$ at 20 Oe holds only at $T \gg T_c$. Inset (b) displays log-log plot of the power law analysis of low-field magnetic susceptibility, $\chi^{-1}(T) \propto (T - T_C{}^R)^{1-\lambda}$. The back solid lines represent the fit to the experimental data following the power law.

ferromagnets.[33] In the original formulation, Griffiths assumed randomly diluted Ising ferromagnets with nearest-neighbor exchange bonds of strength J and 0 distributed with a probability p and $1 - p$, respectively. Long range FM order is established only above a percolation threshold ($p > p_c$) in a reduced T_C, which is below the ordering temperature for an undiluted system, termed as Griffiths temperature T_G. In doped manganites, quenched disorder that arises from the A site disorder is the reason for the random distribution of cations and the consequent random dilution. In a similar fashion, the site disorder in double perovskites can lead to random dilution of the B lattice. The negative curvature of $1/\chi(T)$ in Fig. 4 is observed to diminish in magnitude as magnetic field increases from 20 Oe to 40 kOe. This trend of $1/\chi(T)$ conforms to the general features of a GP phase where inverse susceptibility deviates from Curie–Weiss (CW) description at $T \rightarrow T_c$ and is suppressed at higher magnetic field. In Fig. 4(a), we identify T_G (∼ 164 K) as the characteristic Griffiths temperature where $1/\chi(T)$ commences to deviate from CW description. The low-field magnetic susceptibility in the Griffiths phase follows the power law behavior, $\chi^{-1}(T) \propto (T - T_C^R)^{1-\lambda}$, where λ is the magnetic susceptibility exponent the value of which lies in the range $0 < \lambda < 1$. The magnetic susceptibility of Tb_2NiMnO_6 at $H = 20$ Oe was analyzed using the power law with great care to avoid an incorrect estimation of T_C^R; this can lead to erroneous values of λ. Recent literature that offers a better protocol to perform the analysis was adopted to estimate T_C^R and λ in the purely paramagnetic region.[20,21] Following the procedure reported in literature,[19,20] we first estimated the value of T_C^R in the purely paramagnetic region above T_G. A value of 56 K for T_C^R was estimated in this way that can be compared with that obtained by Zhou *et al.*[20] Using this value of T_C^R, fitting was performed in the GP regime to obtain a value of 0.88 for λ. The result of the analysis is presented in Fig. 4(b) plotted as $\log(1/\chi)$ versus $t_m = (T - T_C^R)/T_C^R$. In the high temperature regime, we obtained $\lambda = 0.08$, signifying that the system has entered a completely paramagnetic phase. The Curie–Weiss analysis of the data above 200 K resulted in effective moment value of $\mu_{eff} = 14.1\ \mu_B$. The spin-only moments of Ni and Mn assuming the combination of Mn^{4+} ($3d^3$, $S = 3/2$)

and Ni^{2+} ($3d^8$, $S = 1$) yields $\mu_{eff} = 4.79\ \mu_B$, and the combination of Mn^{3+} ($3d^4$, $S = 2$) and Ni^{3+} ($3d^7$, $S = 3/2$) results in $\mu_{eff} = 6.24\ \mu_B$. Assuming the rare earth paramagnetic moment to be 9.7 μ_B,[16] the calculated paramagnetic effective moment is ~15.07 μ_B for the Mn^{3+}/Ni^{3+} combination and 14.53 μ_B for the Mn^{4+}/Ni^{2+} combination. A comparison with the experimentally observed value for effective moment suggests that the cationic combination in Tb_2NiMnO_6 is Mn^{4+}/Ni^{2+}. The $1/\chi(T)$ plot at an applied magnetic field of 20 Oe and the corresponding CW fit are presented in Fig. 4(a).

The isothermal magnetization plots of TNMO at 5, 10, and 50 K are illustrated in Fig. 5(a). The qualitative nature of the curves are different from the metamagnetic features observed at low temperatures by Troyanchuk *et al.* in $TbNi_{0.5}Mn_{0.5}O_3$.[34] The saturation magnetization $M_{sat} = 13.5\ \mu_B$ at the highest applied field of 70 kOe is lower than the theoretical value of 23.2 μ_B, which is calculated as $2gJ + 5.2\mu_B$ where, g is the Landé g-factor, J is the total angular momentum, and 5.2 μ_B is the effective Ni-Mn spin-only moment value.[16] In La_2NiMnO_6, the saturation magnetization at highest applied field is reported as 4.57 μ_B, which is close to the theoretical value of 5 μ_B (Ref. 35), but the value of M_{sat} has been observed to vary with the preparation method.[10]

One of the basic characteristics of Griffiths phase is the existence of finite-size FM correlated spins but with no static long-range magnetization that can be verified through the Arrott plots. In Fig. 5(b), we present the Arrott plots—M^2 versus H/M plots—derived from magnetization isotherms at 90, 110, and 120 K. The solid lines in Fig. 5(b) are linear fits to the high-field region extrapolated to the axes so as to obtain the spontaneous magnetization. We observed no spontaneous magnetization in the temperature region close to T_c. The Arrott plots display positive slope, characteristic of second-order phase transitions as prescribed by the Banerjee criterion.[36,37] Generally, the M^2 versus H/M plots are linear for homogeneous ferromagnets,[38] and a deviation from linearity is suggestive of inhomogeneous behavior. The presence of inhomogeneous magnetism in Tb_2NiMnO_6 is confirmed in Fig. 6, where FCW and FCC curves at an applied field of 20 Oe exhibit prominent hysteresis. Similar hysteresis behavior of the FCC and FCW arms has been reported in magnetically phase-separated $La_{0.5}Ca_{0.5}MnO_3$.[39]

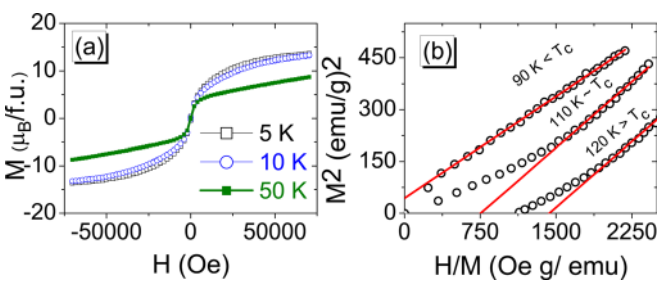

FIG. 5. (Color online) (a) The magnetization plots at 5, 10, and 50 K. (b) The Arrott plots (M^2 vs H/M) at different temperatures below and above T_c. The straight lines are the linear fits to the high-field region in the plot. No spontaneous magnetization is observed in the temperature range near T_c supporting the Griffiths phase-like characteristics.

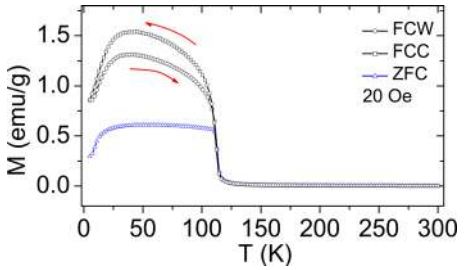

FIG. 6. (Color online) The FCC and FCW cycles at 20 Oe showing a prominent hysteresis of the first-order type resulting from the ferromagnetic clusters that form below T_c.

The structural distortions resulting from the substitution of a smaller rare earth Tb at the R site can couple with the spin system, the signature of which is discernible in Raman scattering experiments. Hence we performed Raman scattering experiments on Tb_2NiMnO_6. The experimentally observed scattering intensity as a function of Raman shift is plotted in Fig. 7(a) for different temperatures. In Fig. 7(b), the intensity at 298 K is plotted as a function of Raman shift and along with deconvoluted peaks assuming Lorenzian peak shapes. Following earlier reports[7,23] which established the similarity of Raman spectra of double perovskite La_2NiMnO_6 with orthorhombic $LaMnO_3$, we assign the respective peaks at 645 cm^{-1} and 490 cm^{-1} to *stretching* and *anti-stretching* vibrations of $(Ni/Mn)O_6$ octahedra.[23] Lattice dynamical calculations attribute mixed character to the 490 cm^{-1} mode that involves both anti-stretching and bending vibrations, whereas the 645 cm^{-1} mode is purely a stretching mode.[24] The Raman spectra of Tb_2NiMnO_6 are similar to that of Pr_2NiMnO_6, which also crystallizes in monoclinic $P2_1/n$ symmetry.[26] The temperature dependence of phonon frequencies, $w(T)$, are shown in Fig. 8(a) along with curve fits assuming a standard[40] anharmonic dependence of phonon modes, $w_{anh}(T) = w_0 - C[1 + 2/(e^{\hbar\omega/k_BT} - 1)]$, where,

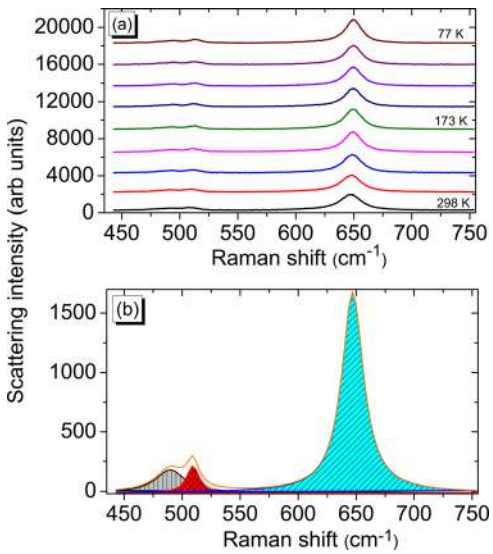

FIG. 7. (Color online) (a) Observed Raman scattering intensity curves of Tb_2NiMnO_6 at different temperatures. (b) The intensity at 298 K as a function of Raman shift, displaying peaks at ~650 cm^{-1}, 510 cm^{-1}, and 490 cm^{-1} (thick line). The shaded areas represent a curve-fit to the observed spectrum using Lorenzian line shape.

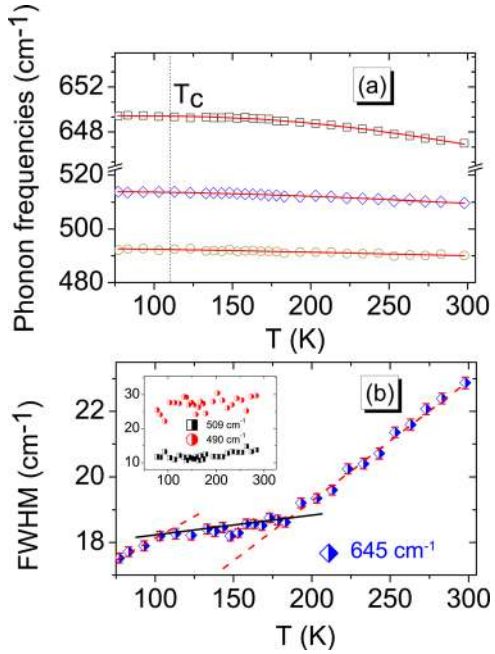

FIG. 8. (Color online) (a) The temperature variation of phonon frequencies in Tb_2NiMnO_6. The solid line is the fit according to the anharmonic phonon-phonon scattering. A vertical black dotted line marks the position of $T_c \cong 111$ K. (b) The FWHM for the peak at 645 cm^{-1} calculated from the experimental Raman intensity as a function of temperature. Note the three different slopes in three different temperature ranges. The red dashed line show typical behavior of FWHM, whereas the solid line represents the anomalous region. The inset displays curves that correspond to peaks at 490 and 509 cm^{-1}; these do not show a slope change.

w_0 is the temperature-independent part of linewidth, C is a constant determined from curve-fit, $\hbar\omega$ is the phonon energy, and k_B is the Boltzmann constant. RMnO$_3$ perovskites, which are A type antiferromagnets, and ferromagnetic double perovskites like La_2NiMnO_6 (LNMO) and La_2CoMnO_6 (LCMO) exhibit magnetic-order-induced phonon renormalization.[24,25,41–43] These systems display mode softening and a deviation from the $w_{anh}(T)$ dependence of phonon frequencies below T_c. However, in RMnO$_3$ systems with an incommensurate magnetic structure (R = Eu, Tb, or Y), no mode softening is observed.[41] However, the data on Tb_2NiMnO_6 yield a reasonably good fit to the standard expression for anharmonic dependence of phonons, showing that the predominant effects in the phonon spectrum are anharmonic. The reduction in spin-phonon coupling is correlated to the size of the R ion as strength of spin-phonon coupling shows a decreasing trend with reduction in rare earth size as reported in the case of Pr_2NiMnO_6.[26] In Fig. 8(b), the temperature variation of full-width-at-half-maximum (FWHM) for pure *stretching* mode at 645 cm^{-1} is plotted. The linewidth of phonon is a measure of the phonon lifetime and is determined by temperature-dependent scattering from lattice defects or phonons. For Tb_2NiMnO_6, as is clear from Fig. 8(b), we observe three different regions in FWHM with discontinuities at $T \sim 110$ K and at 180 K. Note that the discontinuities occur at the same value of temperature where the deviation from perfect CW description occurs in the $1/\chi(T)$ curves. This indicates a close correlation between magnetism and the lattice in Tb_2NiMnO_6.

To summarize the results, we have refined the crystal structure of Tb_2NiMnO_6 in monoclinic $P21/n$ space group that allows for a Ni^{2+}/Mn^{4+} cationic arrangement. The estimated bond distances and the BVS values indicate a nearly ordered B site structure. The down-turn of $1/\chi(T)$ curves from Curie–Weiss behavior, which decreases with the application of magnetic field, is reminiscent of Griffiths phase in disordered systems. The presence of GP in Tb_2NiMnO_6 is further supported by the power-law analysis of $1/\chi(T)$ and the Arrott plots. On a microscopic level, parameters like the magnetic correlation length (ξ) derived from small-angle neutron scattering experiments can further illuminate about the Griffiths phase.[44] For a conventional FM phase transition, $\xi(T)$ displays a gradual increase from zero at high T, then diverges as $T \rightarrow T_c$, whereas in the presence of spin correlations, it shows a sharp increase at the temperature where the clusters emerge. Electron spin resonance (ESR) studies also have been successfully employed to study the GP phase in disordered manganites.[45] At this point, it is instructive to compare the case of La_2NiMnO_6 in which the short range ferromagnetic correlations above T_c have been studied through x ray magnetic circular dichroism,[14] critical behavior,[46] and ESR.[15] Contrary to the case of Tb_2NiMnO_6, a positive deviation of $1/\chi(T)$ from CW description was observed. However, it has been demonstrated that the degree of antisite disorder is a function of the kind of cation at the R site and can be influenced through doping.[47] Analysis of the Raman scattering data showed that in contrast to the behavior seen in other DP like La_2NiMnO_6, magnetic-order-induced mode softening is not observed in Tb_2NiMnO_6. Normally, FWHM of Raman linewidth decreases with temperature as indicated by the dashed line in Fig. 8(b). However, we observe a marked deviation from linear behavior below about 180 K, extending until T_c. In this region, FWHM shows a plateau-like region (black solid line in Fig. 8(b)). The anomalous plateau-like behavior of TNMO is suggestive of increase in phonon lifetime, which originates from the disorder in the system that strongly couples the magnetic and lattice degrees of freedom. The antisite disorder leads to additional antiferromagnetic exchange interactions between Ni-Ni and Mn-Mn. It is significant to note that the range of temperature where deviation from linearity in FWHM occurs (Fig. 8(b)) coincides with the range over which $1/\chi(T)$ deviates from CW description (Fig. 5). Our study projects that Raman scattering can be used as a tool for the characterization of materials exhibiting magneto-lattice coupling effects. The temperature variation of FWHM for other frequencies (presented in Fig. 8(b)) dso not show slope changes; this points toward strong spin-phonon coupling present in the case of symmetric modes like the *stretching* mode. The role of Tb magnetism in Tb_2NiMnO_6 is not significant because ESR studies have shown that the Ni-Mn sublattice interacts weakly with the rare earth.[16] However, the small cationic radius of Tb has a marked impact on structural distortions and contributes to the spin-lattice coupling leading to stronger magnetocapacitive effects.[1] This motivates us to investigate further the magneto-dielectric properties of this compound in detail with emphasis on multiferroism in double perovskites.

IV. CONCLUSIONS

We observe Griffiths phase-like features in the magnetic properties of double perovskite Tb_2NiMnO_6 where the smaller rare earth size of Tb influences the spin-phonon coupling. The value estimated for the inverse susceptibility exponent λ along with the absence of spontaneous magnetization observed through Arrott plots testify the inhomogeneous nature of magnetism in this material and confirm the Griffiths phase-like features. The observed features arise from the site disorder at the *B* site supplemented by the lattice distortions brought about by the smaller radius of Tb. No mode softening of phonon frequencies is observed in Tb_2NiMnO_6; this is qualitatively different from the observation in other double perovskites with a non-magnetic rare earth. Thus we conclude that the magnetic and lattice properties of $R_2BB'O_6$ where *R* is a magnetic rare earth are different from those of the non-magnetic counterparts.

ACKNOWLEDGMENTS

S.E. wishes to thank Department of Science and Technology, India, for financial support through project grants.

[1]N. S. Rogado, J. Li, A. W. Sleight, and M. A. Subramanian, Adv. Mater. **17**, 2225 (2005).
[2]C. L. Bull, D. Gleeson, and K. S. Knight, J. Phys.: Condens. Matter **15**, 4927 (2003).
[3]H. Das, U. V. Waghmare, T. Saha-Dasgupta, and D. D. Sarma, Phys. Rev. Lett. **100**, 186402 (2008).
[4]D. J. Singh and C. H. Park, Phys. Rev. Lett. **100**, 087601 (2008).
[5]S. Kumar, G. Giovannetti, J. van den Brink, and S. Picozzi, Phys. Rev. B **82**, 134429 (2010).
[6]M. Hashisaka, D. Kan, A. Masuno, T. Terashima, M. Takano, and K. Mibu, J. Magn. Magn. Mater. **310**, 1975 (2007).
[7]H. Guo, J. Burgess, S. Street, A. Gupta, T. G. Calvarese, and M. A. Subramanian, Appl. Phys. Lett. **89**, 022509 (2006).
[8]M. P. Singh, C. Grygiel, W. C. Sheets, P. Boullay, M. Hervieu, W. Prellier, B. Mercey, C. Simon, and B. Raveau, Appl. Phys. Lett. **91**, 012503 (2007).
[9]J. B. Goodenough, Phys. Rev. **100**, 564 (1955).
[10]R. I. Dass, J. Q. Yan, and J. B. Goodenough, Phys. Rev. B **68**, 064415 (2003).
[11]A. S. Ogale, S. B. Ogale, R. Ramesh, and T. Venkatesan, Appl. Phys. Lett. **75**, 537 (1999).
[12]S. M. Zhou, Y. Q. Guo, J. Y. Zhao, S. Y, Zhao, and L. Shi, Appl. Phys. Lett. **96**, 262507 (2010).
[13]M. N. Iliev, H. Guo, and A. Gupta, Appl. Phys. Lett. **90**, 151914 (2007).
[14]H. Guo, A. Gupta, M. Varela, S. Pennycook, and J. Zhang, Phys. Rev. B **79**, 172402 (2009).
[15]S. Zhou, L. Shi, H. Yang, and J. Zhao, Appl. Phys. Lett. **91**, 172505 (2007).
[16]R. J. Booth, R. Fillman, H. Whitaker, A. Nag, R. M. Tiwari, K. V. Ramanujachary, J. Gopalakrishnan, and S. E. Lofland, Mater. Res. Bull. **44**, 1559 (2009).
[17]M. B. Salamon and S. H. Chun, Phys. Rev. B **68**, 014411 (2003).
[18]M. B. Salamon, P. Lin, and S. H. Chun, Phys. Rev. Lett. **88**, 197203 (2002).
[19]W. Jiang, X. Zhou, and G. Williams, Europhys. Lett. **84**, 47009 (2008).
[20]S. Zhou, Y. Guo, J. Zhao, L. He, and L. Shi, J. Phys. Chem. C **115**, 1535 (2011).
[21]A. K. Pramanik and A. Banerjee, Phys. Rev. B **81**, 024431 (2010).
[22]H. Z. Guo, J. Burgess, E. Ada, S. Street, A. Gupta, M. N. Iliev, A. J. Kellock, C. Magen, M. Varela, and S. J. Pennycook, Phys. Rev. B **77**, 174423 (2008).
[23]C. L. Bull and P. F. McMillan, J. Solid State Chem. **177**, 2323 (2004).
[24]M. N. Iliev, M. V. Abrashev, A. P. Litvinchuk, V. G. Hadjiev, H. Guo, and A. Gupta, Phys. Rev. B **75**, 104118 (2007).
[25]M. N. Iliev, M. M. Gospodinov, M. P. Singh, J. Meen, K. D. Truong, P. Fournier, and S. Jandl, J. Appl. Phys. **106**, 023515 (2009).
[26]K. D. Truong, M. P. Singh, S. Jandl, and P. Fournier, J. Phys.: Condens. Matter **23**, 052202 (2011).
[27]H. M. Rietveld, J. Appl. Cryst. **2**, 65 (1969).
[28]J. Rodriguez-Carvajal, Phys. B **192**, 55 (1993).
[29]G. V. Pavan Kumar and C. Narayana, Curr. Sci. **93**, 778, (2007).
[30]R. D. Shannon, Acta. Crystallogr. A **32**, 751 (1976).
[31]A. P. Sazonov, I. O. Troyanchuk, M. Kopcewicz, V. V. Sikolenko, U. Zimmermann, and K. Bärner, J. Phys.: Condens. Matter **19**, 046218 (2007).
[32]C. L. Lu, K. F. Wang, S. Dong, J. G. Wan, J. M. Liu, and Z. F. Ren, J. Appl. Phys. **103**, 07F714 (2008).
[33]R. B. Griffiths, Phys. Rev. Lett. **23**, 17 (1969).
[34]I. O. Troyanchuk, N. V. Samsonenko, E. F. Shapovalova, H. Szymczak, and A. Nabialek, Mater. Res. Bull. **32**, 67 (1997).
[35]J. B. Goodenough, A. Wold, R. J. Arnott, and N. Menyuk, Phys. Rev. **124**, 373 (1961).
[36]S. K. Banerjee, Phys. Lett. **12**, 16 (1964).
[37]J. Mira, J. Rivas, F. Rivadulla, C. Vázquez-Vázquez, and M. A. López-Quintela, Phys. Rev. B **60**, 2998 (1999).
[38]G. Herzer, M. Fähnle, T. Egami, and H. Kronmüller, Phys. Stat. Sol. B **101**, 713 (1980).
[39]R. S. Freitas, L. Ghivelder, P. Levy, and F. Parisi, Phys. Rev. B **65**, 104403 (2002).
[40]M. Balkanski, R. F. Wallis, and E. Haro, Phys. Rev. B **28**, 1928 (1983).
[41]J. Laverdière, S. Jandl, A. A. Mukhin, V. Y. Ivanov, V. G. Ivanov, and M. N. Iliev, Phys. Rev. B **73**, 214301 (2006).
[42]E. Granado, A. García, J. A. Sanjurjo, C. Rettori, I. Torriani, F. Prado, R. D. Sánchez, A. Caneiro, and S. B. Oseroff, Phys. Rev. B **60**, 11879 (1999).
[43]K. D. Truong, J. Laverdière, M. P. Singh, S. Jandl, and P. Fournier, Phys. Rev. B **76**, 132413 (2007).
[44]C. He, M. A. Torija, J. Wu, J. W. Lynn, H. Zheng, J. F. Mitchell, and C. Leighton, Phys. Rev. B **76**, 014401 (2007).
[45]J. Deisenhofer, D. Braak, H. A. Krug von Nidda, J. Hemberger, R. M. Eremina, V. A. Ivan-shin, A. M. Balbashov, G. Jug, A. Loidl, T. Kimura, and Y. Tokura, Phys. Rev. Lett. **95**, 257202 (2005).
[46]X. Luo, B. Wang, Y. P. Sun, X. B. Zhu, and W. H. Song, J. Phys: Condens. Matter **20**, 465211 (2008).
[47]M. García-Hernández, J. L. Martínez, M. J. Martínez-Lope, M. T. Casais, and J. A. Alonso, Phys. Rev. Lett. **86**, 2443 (2001).